Supporting Information

Ultrathin CuNi Nanosheets for CO_2 Reduction and O_2 Reduction Reaction in Fuel Cells

Yibo Yan,[a] Zhengping Zhao,[b] Jun Zhao,[c] Yaohui Xu,[a] Yifan Xu,[a] Yuhan Zhao,[a] Wenfei Tang,[a] and Jong-Min Lee,[c]**

[a]Frontiers Science Center for Flexible Electronics, Xi'an Institute of Flexible Electronics (IFE) and Xi'an Institute of Biomedical Materials & Engineering, Northwestern Polytechnical University, 127 West Youyi Road, Xi'an 710072, China

[b]Zhijiang College, Zhejiang University of Technology, Hangzhou, Zhejiang 310014, China

[c]School of Chemical and Biomedical Engineering, Nanyang Technological University, 62 Nanyang Drive, 637459, Singapore

Corresponding to:
Yibo Yan: iamybyan@nwpu.edu.cn
Jong-Min Lee: jmlee@ntu.edu.sg

Table of contents

Synthesis

Ultrathin hexagonal CuNi nanosheets. 7.7 mg of nickel (II) acetylacetonate dissolved in 15 mL of DMF to achieve 2 mmol/L solution which was mixed with 15 mL of 2 mmol/L copper (II) acetylacetonate in DMF solution. De-ionized water (5 mL) and 2-aminopyrene (76 mg) as ligand were pipetted into the mixed solution. Subsequently, it is magnetically stirred and ultrasonicated for 30 min. Then, this mixed solution was transferred to a Teflon-lined autoclave (50 mL capacity). Such sealed autoclave was put inside oven (130 ℃) heating for 3 hours, before cooling to room temperature. Ethanol and acetone were utilized to wash the product sample several times and centrifuged for separation. Precipitate product was conserved in ethanol to keep a liquid phase protection.

Cu_3Ni, Cu_2Ni, $CuNi_2$, $CuNi_3$ nanosheets preparation: The operational synthesis processes were similar to above-mentioned steps, while the precursor dosage were replaced by 1 mmol/L of nickel (II) acetylacetonate in DMF solution and 3 mmol/L of copper (II) acetylacetonate in DMF solution for the preparation of Cu_3Ni.

For Cu_2Ni nanosheets synthesis, the above-mentioned steps were similar, while the precursor dosage were replaced by 1 mmol/L of nickel (II) acetylacetonate in DMF solution and 2 mmol/L of copper (II) acetylacetonate in DMF solution.

For $CuNi_2$ nanosheets synthesis, the above-mentioned steps were similar, while the precursor dosage were replaced by 2 mmol/L of nickel (II) acetylacetonate in DMF solution and 1 mmol/L of copper (II) acetylacetonate in DMF solution.

For $CuNi_3$ nanosheets synthesis, the above-mentioned steps were similar, while the

precursor dosage were replaced by 3 mmol/L of nickel (II) acetylacetonate in DMF solution and 1 mmol/L of copper (II) acetylacetonate in DMF solution.

For pure Cu or Ni nanosheets synthesis, the above-mentioned steps were similar, while the precursor dosage were replaced by 3 mmol/L copper (II) acetylacetonate or 3 mmol/L of nickel (II) acetylacetonate in DMF solution, respectively.

Characterizations

Transmission electron microscopy (TEM) was observed on JEOL JEM 2100F, and atomic force microscopy (AFM) was performed on Bruker ICON AFM. Elemental mapping was conducted by energy-dispersive X-ray (EDX) spectroscopy on JEOL JEM 2100 F. The X-ray diffraction (XRD) pattern was measured by Bruker AXS D8 diffractometer with typically filtered CuKα radiation (λ=0.15406nm) at 40 mA, 40 kV. The X-ray photoelectron spectroscopy (XPS) and Ultraviolet photoelectron spectroscopy (UPS) were conducted by the Kratos Axis Ultra DLD. The XPS spectra were obtained using the Al K-Alpha hν = 1486.6 eV radiation source with accelerating potential of 13 kV, while the UPS spectra were recorded using a He (I) laser source. The high-angle annular dark-field scanning transmission electron microscopy (HAADF-STEM) was observed by FEI Tecnai F20 TEM at accelerating potential of 200 kV. Metallic contents are identified by the inductively coupled plasma (ICP) of PerkinElmer Avio 500. X-ray absorption near edge structure (XANES) spectra were collected from the QuantumLeap X-ray absorption spectroscopy (Sigray) with synchrotron-like performance. The temperature programed desorption (TPD) of CO employed the ChemiSorb 2720 station.

Electrochemical experiments

Chenhua Electrochemical Station (CHI-760E) working station has been employed for electrochemical tests. An airtight and two-compartment cell was used with our samples as working electrode, and Pt foil was utilized as counter electrode. Ag/AgCl (saturated KCl) was employed as the reference electrode. The electrocatalytic reduction of CO_2 was conducted in 0.5 M $KHCO_3$ electrolyte. This electrolyte was saturated by CO_2 for over 30 min before each CO_2RR test, with CO_2 flow rate kept at 10 mL min^{-1} for each experiment. For the preparation of catalyst ink, 10 mg sample was uniformly suspended in 0.5 mL 5wt% Nafion in ethanol solution. Then 50 μL catalyst ink was dropwise pipetted onto and dried on a Ti mesh. The potential-dependent electrolysis has been performed for 4 h at each potential. The gas products from cathode cell has been linked to online gas chromatography (Agilent GC 6890N-G1540N) armed with thermal conductivity detector (TCD), Molecular Sieve 5A column and Porapak Q column. The liquid phase has been analyzed by liquid chromatography (Agilent LC-MS 6130). The theoretical equation for all measurements using Ag/AgCl reference converting to the RHE reference electrode is E (*vs.* RHE) = E (*vs.* Ag/AgCl) + 0.21 V + 0.0591×pH.

The oxygen reduction reaction (ORR) polarization tests were measured in O_2-saturated 0.1 M KOH using a rotating disk electrode (RDE) system at rotating rate of 1600 rpm and scan rate at 10 mV s^{-1}. Koutecky-Levich plots used different rotation rates for the fitting. Fuel cell measurements employed the fuel cell testing setup system (Arbin Instruments). The membrane electrolyte assembly (MEA) with effective area of 5.0 cm^2 has been developed using catalyst-spray membrane approach. Primarily, catalyst ink

slurry was prepared via ultrasonication of catalyst powder with isopropanol and 5 wt% Nafion for 1 h. Next, the ink slurry was sprayed on one side of the diaphragm membrane to serve as the cathode catalyst layer. Commercial Pt/C (60wt%) was employed as the anode catalyst, and this anode catalyst ink was prepared via similar approach and sprayed on the other side of diaphragm membrane to serve as the anode catalyst layer. The Pt loading on anode was 0.1 mg cm^{-2}. Gas diffusion layers (GDLs) were prepared based on carbon paper (TGP-H-060, Toray) pre-immersed in acetone (12 h) to remove contaminants before treating with 5 wt% PTFE solution, and annealing (at 350 °C) for 1 h to acquire a dry PTFE loading of 15 wt% on carbon paper. Next, the mixture of carbon powder (VulcanXC-72, Cabot), 5 wt% PTFE dispersion and isopropanol were ultrasonicated for 30 min. Then this ink slurry was sprayed on one side of carbon paper to form microporous layer (MPL) before annealing at 350 °C for 1 h. PTFE content was 15 wt% and carbon powder loading was 4.0 mg cm^{-2} on MPL. Ultimately, the fuel cell was assembled using as-prepared MEAs and two pieces of GDLs on both sides through hot press at 120 °C for 5 min with pressure of 600 lbs.

For H_2-air fuel cell test, hydrogen (99.999%) was fed into anode at 150 mL min^{-1}, while compressed air was fed into cathode at 300 mL min^{-1}. Both cell and gas humidifier were kept at 80 °C during tests. Before measurements, the single fuel cell was activated using continuous discharge mode (>3 h) until stability was attained. The cells working condition was 80 °C with hydrogen humidity (RH) at 100%. The anode and cathode back pressures are both 30 psi.

For air-breathing fuel cell, MEA was prepared through the same protocol as above,

using the air-breathing fuel cell test setup on Fuel Cell Testing System (Sunlaite TE201), at air-conditioned 26 °C. The cathode of fuel cell was connected to the atmosphere directly gaining the oxygen from air and the dry hydrogen flow rate was adjusted dependent on the discharge current.

Computation methods

Automated density functional theory (DFT) framework has been established using multiple Python and shell software packages. Pymatgen[1] was employed to compute all facets with Miller indices from -2 to 2 and all symmetrically different facets. Pymatgen also performed surface Delaunay triangulation to compute adsorption sites. Vienna ab initio simulation package (VASP) [2] together with the Perdew–Burke–Ernzerhof (PBE) [3] are applied for DFT calculations. DFT results were utilized by machine learning workflow for prediction of CO adsorption and H adsorption energies.[4] The DFT mapping is performed with VASP [2] implemented in atomic simulation environment (ASE).[5] The 2-dimensional activity and selectivity volcano plots were obtained from the code by Liu et al.[6] Gibbs free energy changes were obtained in a proton-coupled electron transfer (PCET) process using a well-recognized computational hydrogen electrode (CHE) model.[7] Zero-point energies (ZPE) and the vibrational influence on entropy for various adsorbates were considered within a well-constructed harmonic oscillator approximation.[8] To remain balance between efficiency and computation accuracy, the DFT Semi-core Pseudo-potential (DSPP) has been utilized as a core treatment. The double numerical plus polarization has been used as a basis set. And Brillouin zone has been sampled with a 2 × 2 × 1 Monkhorst-Pack point.[9] The Gaussian

smearing technique (0.005 Ha default smearing width) has been utilized to accelerate convergence. The self-consistent-field (SCF) convergence criteria (set as 1.0×10^{-6} Ha), energy convergence criteria (set as 2.0×10^{-5} Ha), maximum force convergence criteria (set as 0.004 Ha/Å), the maximum displacement criteria (set as 0.005 Å) have been employed, respectively.

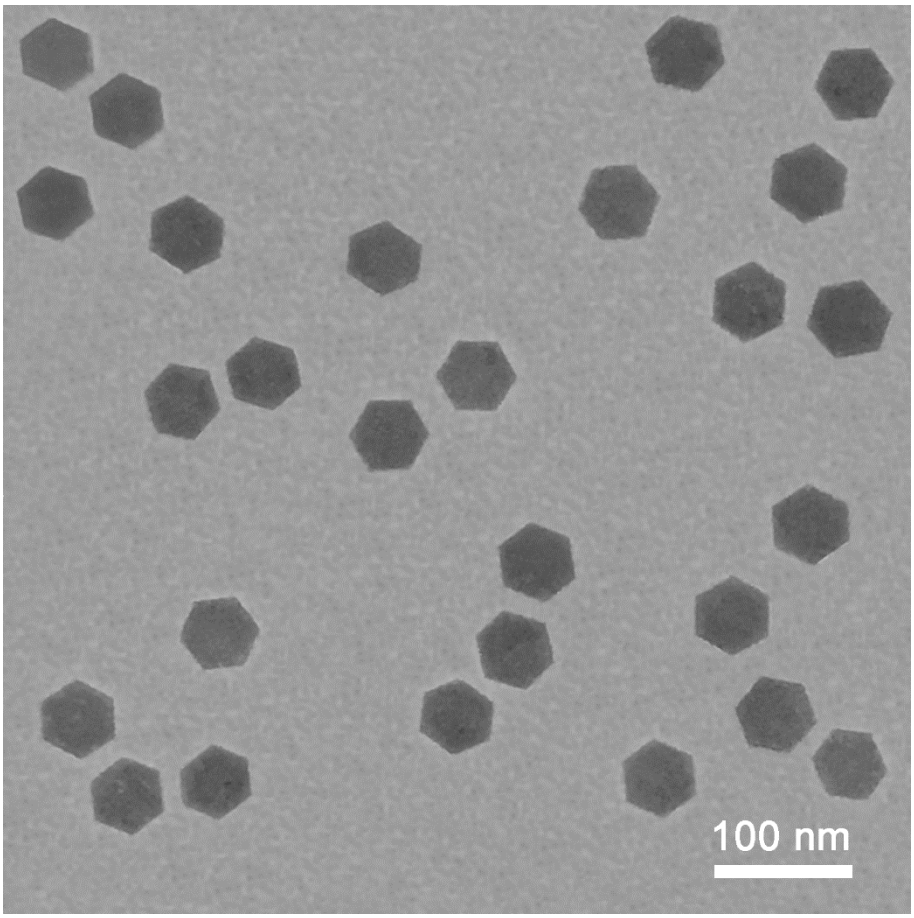

Figure S1 TEM image observation of the ultrathin hexagonal Cu_3Ni nanosheets.

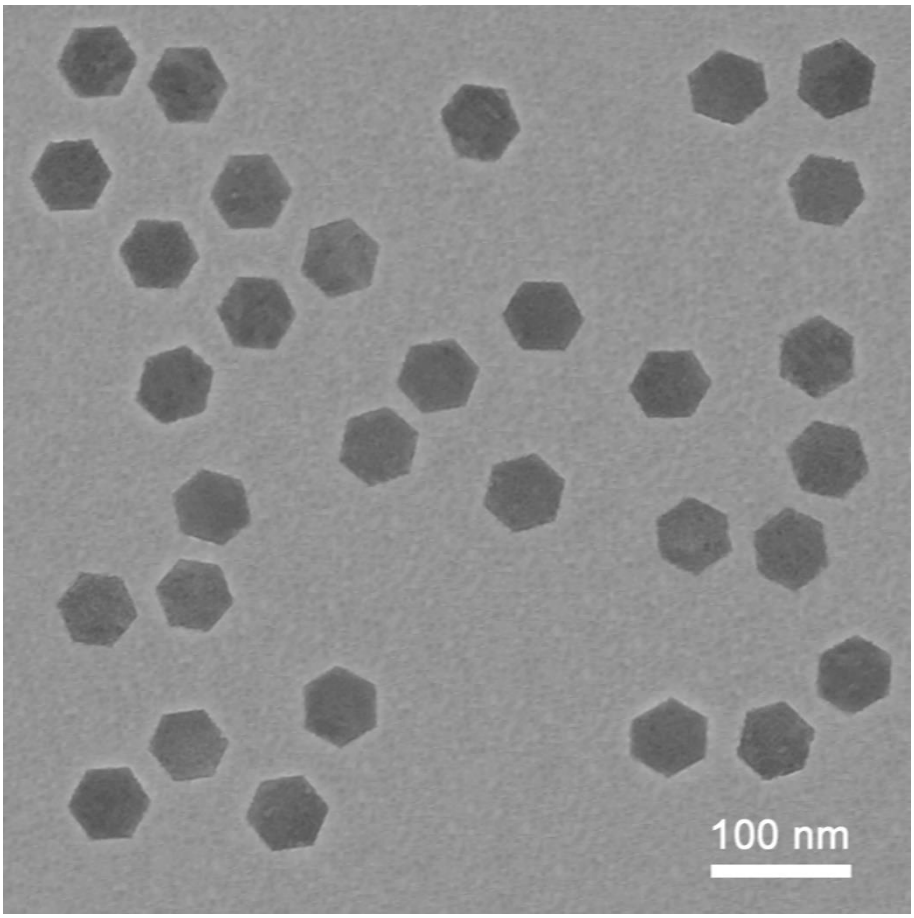

Figure S2 TEM image observation of the ultrathin hexagonal Cu_2Ni nanosheets.

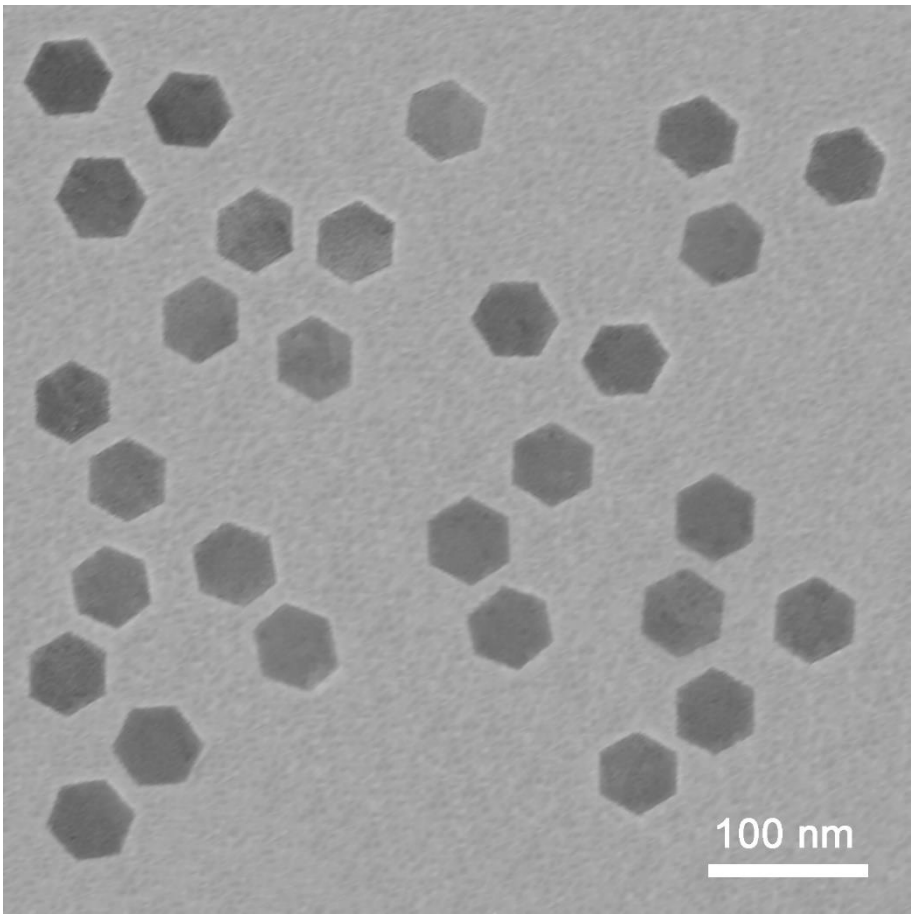

Figure S3 TEM image observation of the ultrathin hexagonal $CuNi_2$ nanosheets.

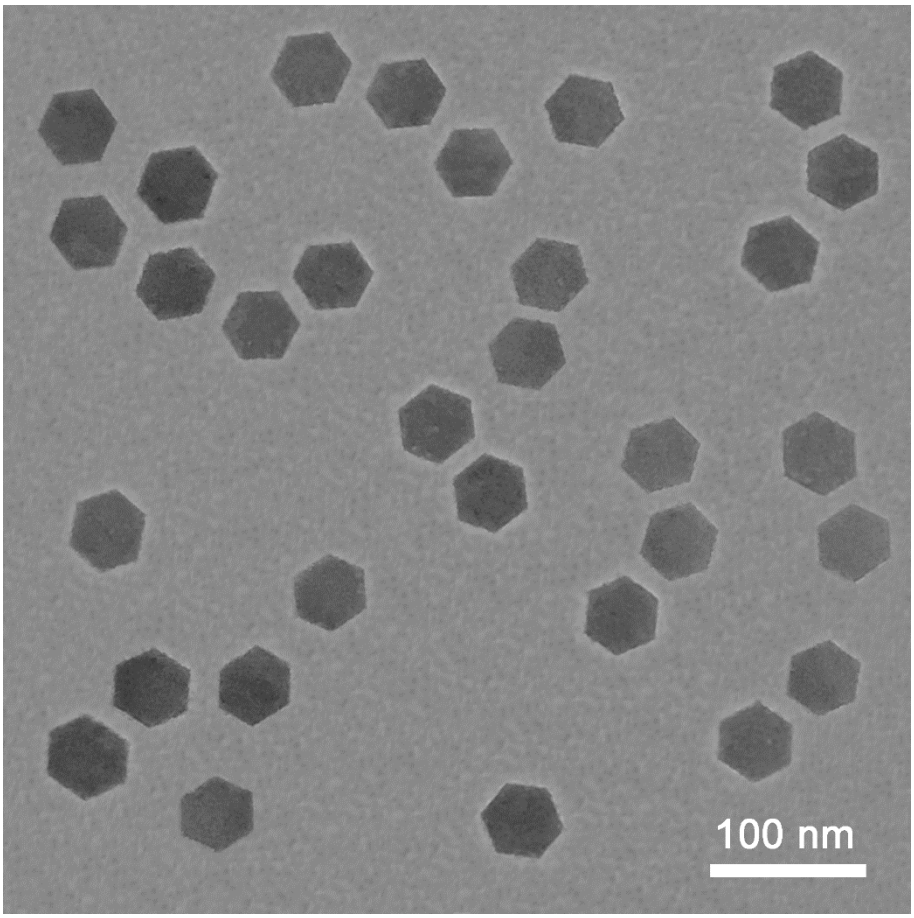

Figure S4 TEM image observation of the ultrathin hexagonal $CuNi_3$ nanosheets.

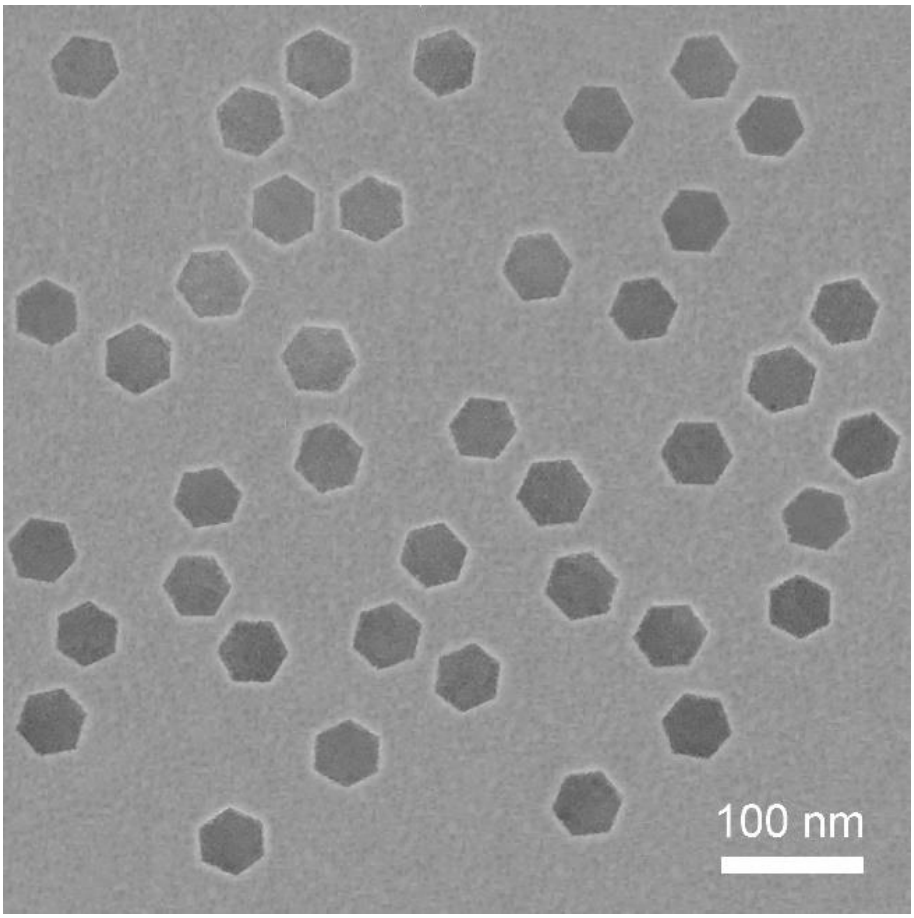

Figure S5 TEM image observation of the ultrathin hexagonal pure Cu nanosheets.

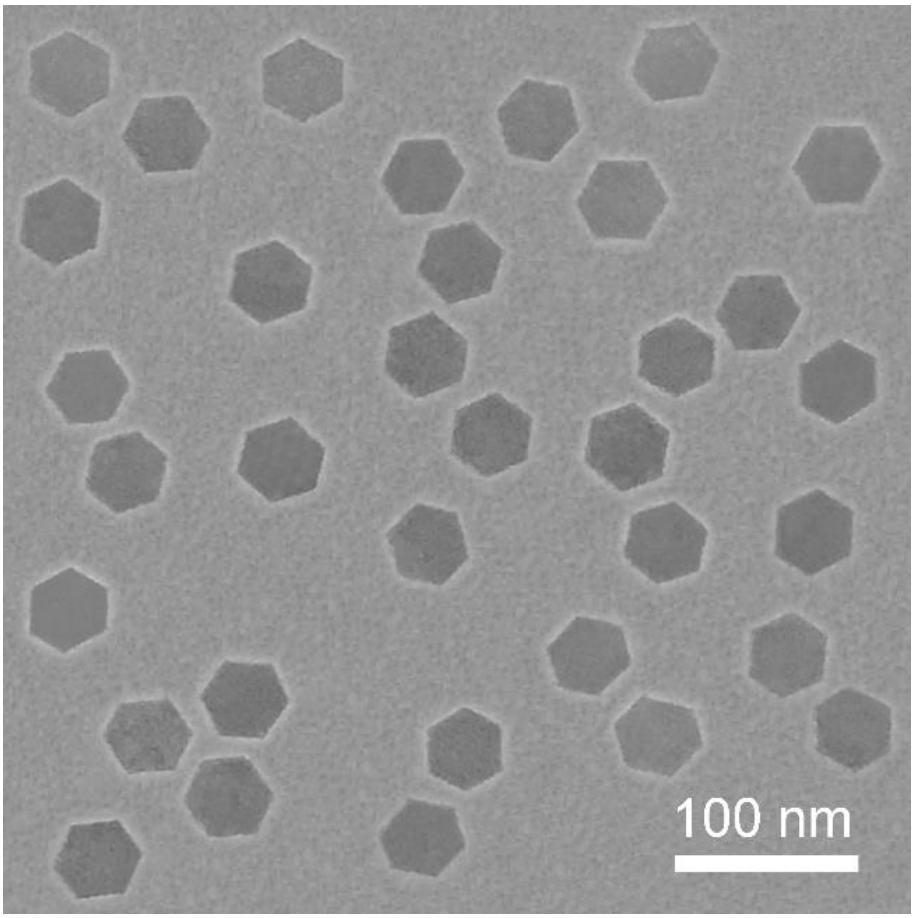

Figure S6 TEM image observation of the ultrathin hexagonal pure Ni nanosheets.

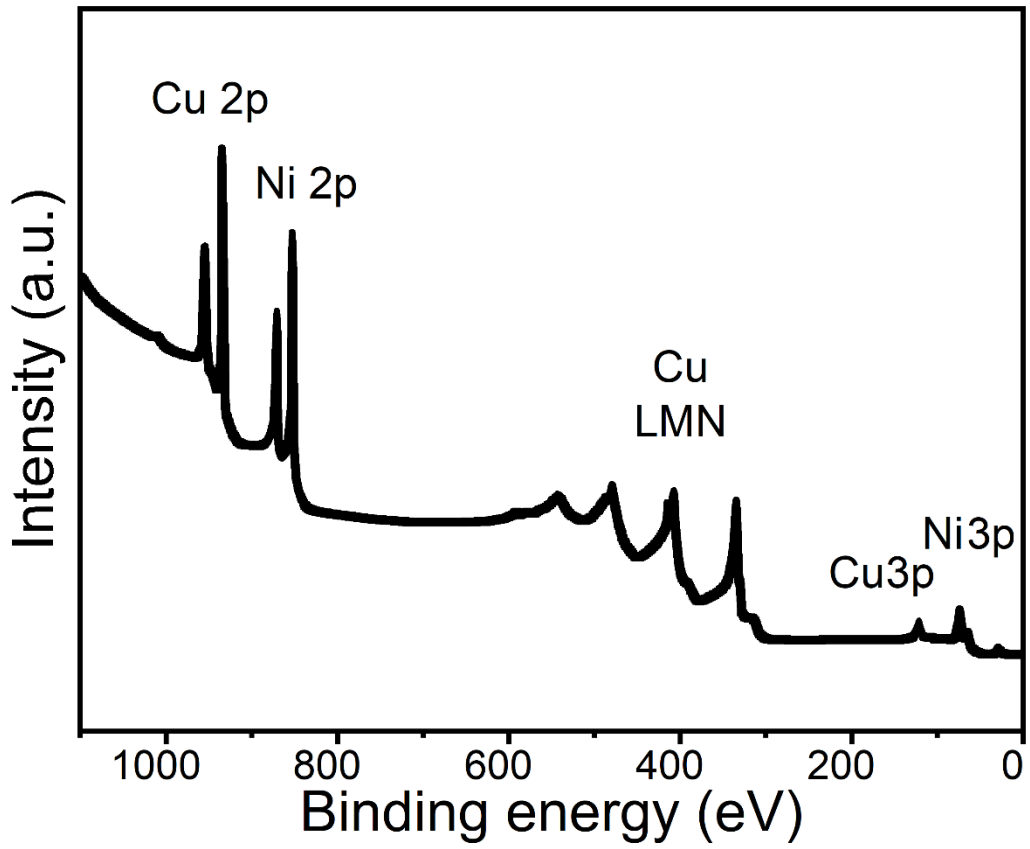

Figure S7 Overall XPS spectrum of the ultrathin hexagonal CuNi nanosheets.

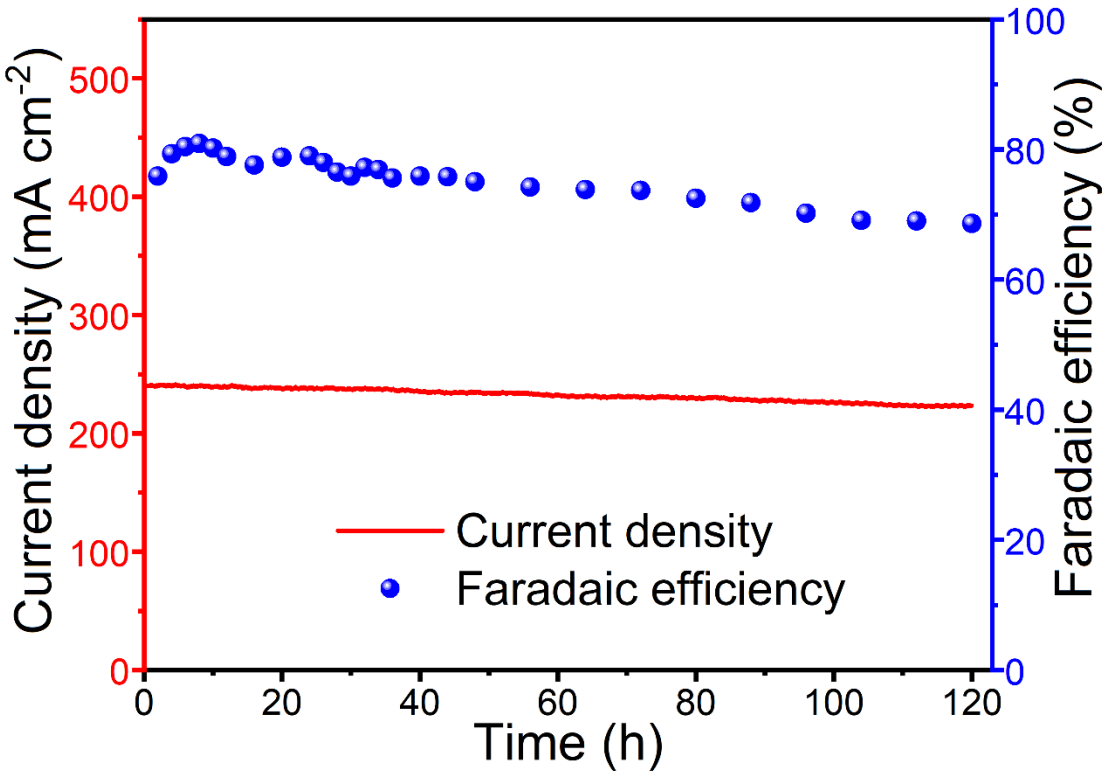

Figure S8 Total current density (red line) and the faradaic efficiency for ethylene (blue ball) using CuNi electrocatalyst for the electrolysis duration of 120 h.

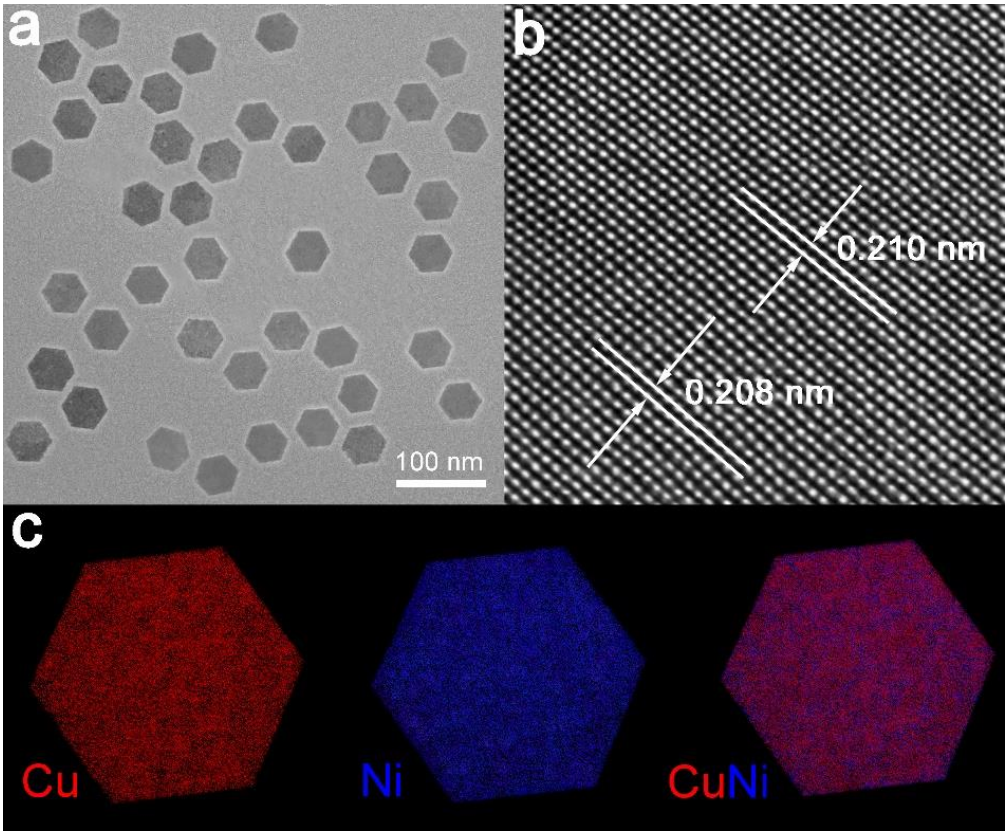

Figure S9 Observation of the CuNi hexagonal nanosheets after electrochemical testing and characterized by TEM (a), HRTEM (b), and EDX elemental mapping (c). Different from single crystal, the presence of Cu and Ni distribution causes tiny distortion of lattice which lead to tiny shift of XRD peaks (according to Bragg's law). The EDX characterization exhibits the almost uniform distribution of the Cu and Ni atoms.

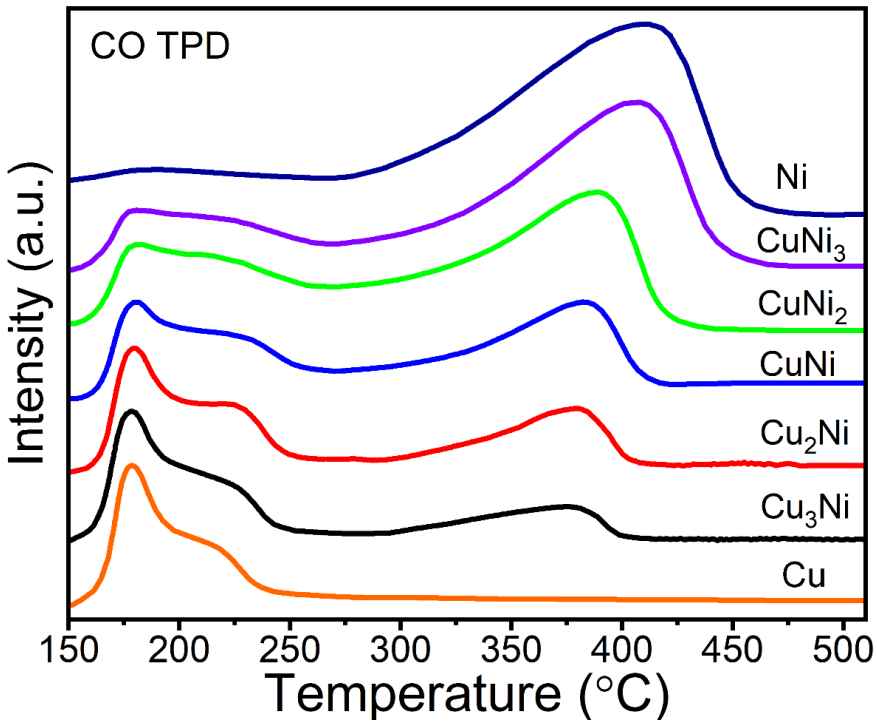

Figure S10 Temperature programmed desorption (TPD) of CO from the surface of Cu, Cu_3Ni, Cu_2Ni, CuNi, $CuNi_2$, $CuNi_3$ and Ni electrocatalysts, respectively.

REFERENCES

1. Ong, S. P.; Richards, W. D.; Jain, A.; Hautier, G.; Kocher, M.; Cholia, S.; Gunter, D.; Chevrier, V. L.; Persson, K. A.; Ceder, G., Python Materials Genomics (pymatgen): A robust, open-source python library for materials analysis. *Computational Materials Science* **2013,** *68*, 314-319.
2. Kresse, G.; Furthmuller, J., Efficient iterative schemes for ab initio total-energy calculations using a plane-wave basis set. *Physical Review B* **1996,** *54* (16), 11169-11186.
3. Perdew, J. P.; Burke, K.; Ernzerhof, M., Generalized Gradient Approximation Made Simple. *Physical Review Letters* **1996,** *77* (18), 3865-3868.
4. Zhong, M.; Tran, K.; Min, Y.; Wang, C.; Wang, Z.; Dinh, C.-T.; De Luna, P.; Yu, Z.; Rasouli, A. S.; Brodersen, P.; Sun, S.; Voznyy, O.; Tan, C.-S.; Askerka, M.; Che, F.; Liu, M.; Seifitokaldani, A.; Pang, Y.; Lo, S.-C.; Ip, A.; Ulissi, Z.; Sargent, E. H., Accelerated discovery of CO2 electrocatalysts using active machine learning. *Nature* **2020,** *581* (7807), 178-183.
5. Larsen, A. H.; Mortensen, J. J.; Blomqvist, J.; Castelli, I. E.; Christensen, R.; Dułak, M.; Friis, J.; Groves, M. N.; Hammer, B.; Hargus, C., The atomic simulation environment—a Python library for working with atoms. *Journal of Physics: Condensed Matter* **2017,** *29* (27), 273002.
6. Liu, X.; Xiao, J.; Peng, H.; Hong, X.; Chan, K.; Nørskov, J. K., Understanding trends in electrochemical carbon dioxide reduction rates. *Nature communications* **2017,** *8* (1), 1-7.
7. Nørskov, J. K.; Rossmeisl, J.; Logadottir, A.; Lindqvist, L.; Kitchin, J. R.; Bligaard, T.; Jónsson, H., Origin of the Overpotential for Oxygen Reduction at a Fuel-Cell Cathode. *The Journal of Physical Chemistry B* **2004,** *108* (46), 17886-17892.
8. Xie, M. S.; Xia, B. Y.; Li, Y.; Yan, Y.; Yang, Y.; Sun, Q.; Chan, S. H.; Fisher, A.; Wang, X., Amino acid modified copper electrodes for the enhanced selective electroreduction of carbon dioxide towards hydrocarbons. *Energy & Environmental Science* **2016,** *9* (5), 1687-1695.
9. Monkhorst, H. J.; Pack, J. D., SPECIAL POINTS FOR BRILLOUIN-ZONE INTEGRATIONS. *Physical Review B* **1976,** *13* (12), 5188-5192.